Universidad de Alcalá
BIBLIOTECA

Document downloaded from the institutional repository of the University of Alcala: http://ebuah.uah.es/dspace/

This is a postprint version of the following published document:

Yang, L., Psychogiou, D. & Gómez García, R. 2022, "High-order input-reflectionless quasi-elliptic-type wideband bandpass filter using dual-mode slotline resonator", in 2022 Asia-Pacific Microwave Conference (APMC), Yokohama, Japan, 2022, pp. 455-457.

Available at http://dx.doi.org/10.23919/APMC55665.2022.9999911

© 2022 IEEE. Personal use of this material is permitted. Permission from IEEE must be obtained for all other users, including reprinting/republishing this material for advertising or promotional purposes, creating new collective works for resale or redistribution to servers or lists, or reuse of any copyrighted components of this work in other works.

(Article begins on next page)

This work is licensed under a

Creative Commons Attribution-NonCommercial-NoDerivatives 4.0 International License.

High-Order Input-Reflectionless Quasi-Elliptic-Type Wideband Bandpass Filter Using Dual-Mode Slotline Resonator

Li Yang[#1], Dimitra Psychogiou[*2], Roberto Gómez-García[#3]

[#]*Department of Signal Theory and Communications, University of Alcalá, Alcalá de Henares, Madrid, 28871, Spain*

[1]li.yang@uah.es,[3]roberto.gomez.garcia@ieee.org

[*]*School of Engineering, University College Cork, Cork, T12 K8AF Ireland*

[2]dpsychogiou@ucc.ie

***Abstract*—A high-order input-reflectionless quasi-elliptic-type wideband bandpass filter (BPF) that exploits a complementary-diplexer-based topology is reported. Firstly, a fourth-order wideband microstrip-to-microstrip vertical transition employing a dual-mode slotline resonator as the reflective-type BPF channel is designed. It features a sharp-rejection BPF response with two close-to-passband transmission zeros (TZs). To attain broadband input-reflectionless behavior, a shunt resistively-terminated microstrip π-shape network is used as the absorptive bandstop-filter (BSF) channel. The RF theoretical operational principle of the conceived broadband BPF is detailed. Compared to prior-art high-order input-/two-port-reflectionless wideband BPFs, the proposed BPF features not only improved passband flatness at the passband edges, but also relatively-high stopband power-attenuation levels and power-absorption ratios. For experimental-validation purposes, a two-layer fourth-order BPF microstrip prototype centered at 1 GHz is developed and tested.**

Index Terms — Absorptive filter, bandpass filter (BPF), two-layer structure, reflectionles filter, wideband filter.

I. Introduction

To suppress the unwanted stopband-RF-signal-power echoes so as to guarantee the robust operation of preceding active circuits in RF front-end chains, absorptive/reflectionless bandpass filters (BPFs) need to be incorporated within the RF transceiver [1]. Unlike conventional solutions that use bulky RF isolators or attenuators, more-compact RF front-end chains can be realized with absorptive BPFs. In these BPF devices, the stopband non-transmitted RF-input-signal power reflections are expected to be fully dissipated by the resistive elements inside their lossy circuits [2]. Until now, input-/two-port-absorptive BPFs are mostly realized with three different design methods. These include symmetrical lossy circuits with equal-amplitude but out-of-phase even-/odd-mode sub-networks [3], [4], back-to-back-cascaded quadrature-coupler-based networks [5], and complementary-diplexer-based BPF and lossy bandstop-filter (BSF) channels [6]–[8]. However, most of these BPFs are designed with narrow or moderate bandwidths [3]–[6], and only a few of them feature wideband BPF responses as in [7], [8]. In [7], two-layer two-port-reflectionless wideband BPFs with shunt/in-series resistively-terminated microstrip lines were reported. However, their passband flatness and power-absorption-ratio profiles are poor throughout the stopband-to-passband transitions. Alternative input-reflectionless quasi-elliptic-type wideband BPF schemes

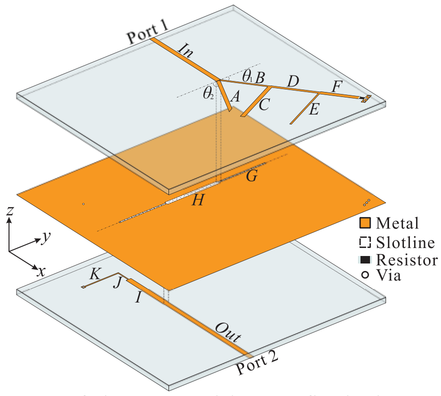

Fig. 1. Layout of the proposed input-reflectionless quasi-elliptic-type wideband BPF using a dual-mode slotline resonator.

were explored in [8] to improve the passband flatness and the sharpness of the power-absorption-ratio profile within the stopband-to-passband transitions. Although a higher-order BPF was engineered in [8] to augment the stopband power-attenuation levels (PALs), it still suffers from some critical drawbacks (e.g., relatively-rounded passband at its edges, high in-band power-insertion-loss levels, and large circuit size). Thus, compact input-reflectionless wideband BPFs with further-improved passband flatness and enhanced stopband PALs are still needed.

In this paper, a compact high-order input-reflectionless wideband BPF is presented. Its BPF channel is realized with a fourth-order quasi-elliptic-type vertical transition built on a dual-mode slotline resonator. Its dissipative BSF channel is shaped by a shunt resistively-terminated fifth-order lowpass-filter-(LPF)-based π-shape network. The proposed BPF exhibits further-improved passband flatness at the band edges and relatively-high stopband power-absorption-ratio profile. Its theoretical foundations and design procedure are detailed. Finally, a demonstrative 1-GHz two-layer input-reflectionless BPF microstrip prototype is manufactured and tested.

II. Theoretical Foundations

The layout of the proposed input-reflectionless wideband BPF in a complementary diplexer-based structure is shown in Fig. 1. Here, its reflective-type BPF channel is built by a fourth-order microstrip-to-microstrip vertical transition.

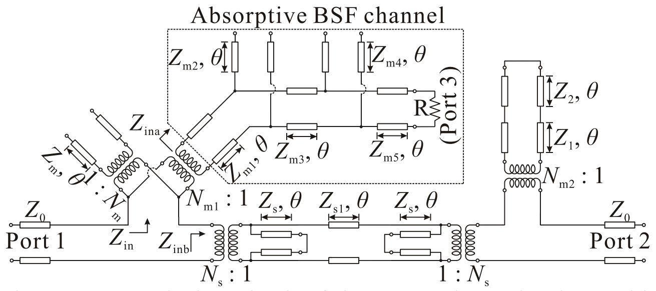

Fig. 2. TL equivalent circuit of the proposed BPF in Fig. 1 with $Z_m = N_m^2 \times Z'_m$, $Z_s = N_s^2 \times Z'_s$, $Z_{m1} = N_{m1}^2 \times Z'_{m1}$, and $Z_1 = N_{m2}^2 \times Z'_1$.

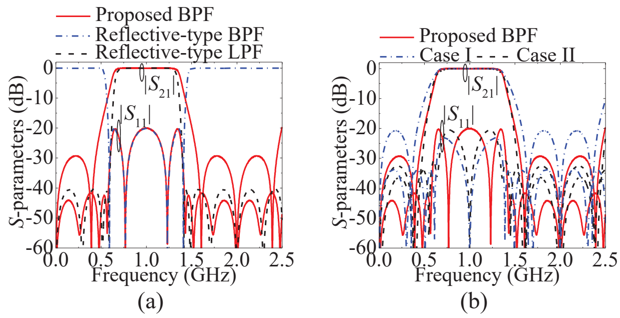

Fig. 3. Theoretical frequency responses of the proposed fourth-order input-reflectionless wideband BPF. (a) Power transmission ($|S_{21}|$) and input-reflection ($|S_{11}|$) responses of the proposed BPF with $z_m = 0.9527$, $z_s = 0.6217$, $z_{s1} = 1.1048$, $z_1 = 0.97$, $z_2 = 1.934$, $z_{m1} = 1.7885$, $z_{m2} = 0.893$, $z_{m3} = 1.613$, $z_{m4} = 1.7938$, and $z_{m5} = 1.0706$. Its relevant reflective-type fourth-order $|S_{11}|$ associated to the pure imaginary F_{BPF} (so that to meet the specified Chebyshev-type equal-ripple BPF response with $L_{A1} = 0.04308$ and $\theta_{c1} = 56.7°$ at $f_{c1} = 0.579$ GHz) and the reflective-type $|S_{11}|$ of the reshaped input-reflectionless LPF resulting from the pure imaginary F_{LPF} (so that to feature the pre-defined Chebyshev-type seventh-order equal-ripple response) are also depicted. (b) Comparison of the $|S_{21}|$ and $|S_{11}|$ responses of the proposed BPF with those of the following BPFs that were reported in [8]: (i) third-order wideband BPF using a resistively-ended π-shaped structure (Case I) and (ii) high-order wideband BPF with two in-series cascaded replicas of third-order wideband BPFs using a resistively-terminated T-junction (Case II).

Compared with the three-pole vertical transition using a half-wavelength resonator, a dual-mode slotline resonator etched on the ground plane is exploited to obtain one more transmission pole. Unlike the in-series open-circuit-ended microstrip resonator, a short-circuit-ended two-section microstrip line is printed on the bottom layer to shape a quasi-elliptic-type response with two close-to-passband transmission zeros (TZs). For the shunt lossy BSF channel, a resistively-terminated microstrip π-shape network is employed to realize a broadband input-reflectionless behavior.

Based on the layout of the proposed wideband BPF, its transmission-line (TL) equivalent circuit are derived as shown in Fig. 2. Here, the impedances of the open-circuit-ended stub, the short-circuit-ended stubs, the cascaded TL section, and the short-circuit-ended two-stage TL sections of the reflective-type BPF channel are Z_m, Z_s, Z_{s1}, Z_1, and Z_2. Whilst, the impedances of the in-series cascaded TL sections and the shunt open-ended stubs of the lossy BSF channel are Z_{m1}, Z_{m2}, Z_{m3}, Z_{m4}, and Z_{m5}. All the stubs and TL sections are set with the same electrical length $\theta = \pi/2$ at the center frequency f_0. R is the resistance of the loaded 50-Ω resistor, and Z_{in}, Z_{ina}, and Z_{inb} are the input impedances of the relevant TL sub-networks. In addition, to quantitatively model the impedance variations of the coupled microstrip and slotline resonators in Fig. 1 during the electromagnetic (EM) simulation, four transformers with different turns ratios of N_m, N_s, N_{m1}, and N_{m2} are used.

Following the detailed design method in [8], the operational principles of the proposed BPF are described. It is initially set as an ideal lossless network, which owns $N_m = N_s = N_{m1} = N_{m2} = 1$. With the derived *ABCD* matrix of the BPF in Fig. 1, the characteristic function F_{BPF} in a composite expression is firstly obtained. By imposing the in-band frequency response of this lossy BPF to meet a specific fourth-order reflective-type Chebyshev equal-ripple response, the pure imaginary part of F_{BPF} (as well as of Z_{in} or Z_{ina}) is considered. As design example, an impedance ratio $Z_1/Z_2 = 0.5015$ is chosen, which leads to two close-to-passband TZs at $0.392f_0$ and $1.608f_0$. The desired four-pole reflective-type Chebyshev equal-ripple BPF response is specified with passband ripple $L_{A1} = 0.04308$ dB and electrical length $\theta_{c1} = 56.7°$ at the lower cut-off frequency $f_{c1} = 0.579$ GHz (or return-loss level of 20.06 dB at $f_0 = 1$ GHz). Hence, the initial set of the normalized impedance values for the proposed BPF are attained as $z_m = 0.5578$, $z_s = 0.8328$, $z_{s1} = 1.1048$, $z_1 = 0.97$, $z_2 = 1.934$, $z_{m1} = 1.789$, $z_{m2} = 0.891$, $z_{m3} = 1.613$, $z_{m4} = 1.7938$, and $z_{m5} = 1.0706$.

On the other hand, by loading a 50-Ω resistor at the output port (Port 2) of the reflective-type BPF channel and removing the terminating resistor at the output port (Port 3) of the absorptive BSF channel, the proposed BPF is reshaped as a lossy seventh-order input-absorptive LPF. Similarly, the calculated characteristic function F_{LPF} of this reshaped input-reflectionless LPF and Z_{inb} are assumed as pure imaginary. Its in-band frequency response is also expected to feature a specific reflective-type seventh-order Chebyshev equal-ripple LPF response, for which the values for the passband ripple $L_{A2} = 0.00041$ dB and the electrical length $\theta_{c2} = 53.406°$ at the lower cut-off frequency $f_{c2} = 0.5934$ GHz are imposed. Based on the initially-determined impedance values that are associated to the specified reflective-type four-pole Chebyshev BPF response, the normalized impedances of the reshaped LPF for the defined seventh-order Chebyshev LPF response are obtained. They are $z_m = 0.9527$, $z_s = 0.6217$, $z_{s1} = 1.1048$, $z_1 = 0.97$, $z_2 = 1.934$, $z_{m1} = 1.8318$, $z_{m2} = 0.8797$, $z_{m3} = 1.613$, $z_{m4} = 1.7938$, and $z_{m5} = 1.0706$. In this context, as shown in Fig. 3(a) and in order to simultaneously fulfil the specified reflective-type Chebyshev equal-ripple four-pole BPF and seven-pole LPF responses under the discussed assumptions, the normalized impedances of the proposed BPF are quantitatively selected with $z_m = 0.9527$, $z_s = 0.6217$, $z_{s1} = 1.1048$, $z_1 = 0.97$, $z_2 = 1.934$, $z_{m1} = 1.7885$, $z_{m2} = 0.893$, $z_{m3} = 1.613$, $z_{m4} = 1.7938$, and $z_{m5} = 1.0706$. Here, only the values of z_{m1} and z_{m2} are slightly adjusted. Fig. 3(b) depicts the theoretical frequency responses of the proposed BPF. They are compared with those of the third-order wideband BPF using a

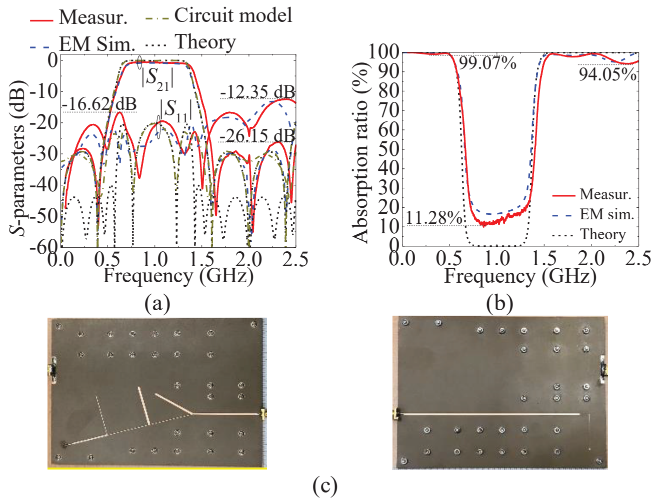

Fig. 4. Frequency responses of the designed fourth-order input-reflectionless wideband BPF prototype with L_{in} = 45, L_{out} = 95, L_A = 28.35, L_B = 29.7, L_C = 28.15, L_D = 29.35, L_E = 29.16, L_F = 28.17, L_G = 27.44, L_H = 31.28, L_I = 27.66, L_J = 6.5, L_K = 23.39, W_A = 1.19, W_B = 0.23, W_C = 1.4, W_D = 0.28, W_E = 0.34, W_F = 0.81, W_G = 0.12, W_H = 0.91, W_I = 1.26, W_J = W_K = 0.16, W_{in} = W_{out} = 1.1 (unit: mm), θ_1 = 75°, and θ_2 = 60°. (a) Theoretical, EM-simulated, circuit model, and measured power transmission ($|S_{21}|$) and input-reflection ($|S_{11}|$) responses. (b) Theoretical, EM-simulated, and measured power-absorption ratios [i.e., $100\times(1-|S_{21}|^2-|S_{11}|^2)$ (%)]. (c) Top/bottom-view photographs of the assembled BPF prototype.

resistively-terminated π-shaped structure (Case I) and the high-order wideband BPF with two cascaded three-order units employing a resistively-loaded T-junction (Case II) that were reported in [8]. As shown, the proposed BPF features improved passband flatness at the band edges and relatively-high PALs with regard to the metrics of Cases I and II.

III. Experimental Results

To verify the viability of the proposed wideband BPF in Fig. 1, a two-layer microstrip prototype is manufactured and tested. A substrate with relative dielectric constant ε_r = 10.2, dielectric thickness h = 1.27 mm, and dielectric loss tangent $\tan(\delta_D)$ = 0.0023 is utilized. To make the EM-simulated results fairly close to the theoretical ones, the proposed BPF is simulated with Z'_m = 47.92 Ω, Z'_s = 49.28 Ω, Z_{s1} = 79.97 Ω, Z'_1 = 46.64 Ω, Z_2 = 93.19 Ω, Z'_{m1} = 85.34 Ω, Z_{m2} = 44.29 Ω, Z_{m3} = 80.99 Ω, Z_{m4} = 76.62 Ω, and Z_{m5} = 56.72 Ω. Thus, compared with the selected values of the normalized-impedance parameters for the theoretical responses, the turns ratios of the used transformers are extracted as N_m = 0.997, N_s = 0.794, N_{m1} = 1.024, and N_{m2} = 1.02. The resistance of the soldered surface-mounted-device resistor is measured as R = 50.1 Ω. Fig. 4(a) plots the theoretical, EM-simulated, circuit model, and measured results. Good agreement among them is observed. The main performance metrics of the measured wideband BPF are as follows: center frequency of 1.035 GHz with minimum in-band power-insertion-loss level of 0.45 dB, 1-dB fractional bandwidth (FBW) of 64.26% and 3-dB FBW of 72.29%, stopband PAL of 26.15 dB, and input power-matching levels above 12.35 dB from DC to 2.5 GHz (i.e., 2.5 f_0). Fig. 4(b) reveals that a measured minimum stopband-power-absorption ratio above 94.05% from DC to 2.56 GHz is attained, whereas the measured minimum in-band power absorption ratio is equal to 11.28% at 0.988 GHz. The photographs of the BPF prototype are shown in Fig. 4(c).

IV. Conclusion

A two-layer fourth-order input-reflectionless wideband BPF using a dual-mode slotline resonator is reported. Its theoretical foundations and RF operational principle have been presented through the detailed description of its design procedure. For validation, a microstrip prototype of a fourth-order input-reflectionless BPF unit has been manufactured and tested.

Acknowledgement

This work was supported in part by the GOT ENERGY TALENT (GET) fellowship programme cofunded by the EU as part of the H2020-MSCA-COFUND programme under Grant Agreement number 754382 and in part by the Spanish Ministry of Science and Innovation (State Research Agency) under Project PID2020-116983RB-I00.

References

[1] Mini-Circuits, Brooklyn, NY., "Reflectionless filters improve linearity and dynamic range," *Microw. J.*, vol. 58, no. 8, pp. 42–50, Aug. 2015.

[2] R. Gómez-García, D. Psychogiou, J.-M. Muñoz-Ferreras, and L. Yang, "Avoiding RF isolators: Reflectionless microwave bandpass filtering components for advanced RF front ends," *IEEE Microw. Mag.*, vol. 21, no. 12, pp. 68–86, Dec. 2020.

[3] M. A. Morgan and T. A. Boyd, "Theoretical and experimental study of a new class of reflectionless filter," *IEEE Trans. Microw. Theory Techn.*, vol. 59, no. 5, pp. 1214–1221, May 2011.

[4] M. A. Morgan and T. A. Boyd, "Reflectionless filter structures," *IEEE Trans. Microw. Theory Techn.*, vol. 63, no. 4, pp. 1263–1271, Apr. 2015.

[5] P. Ma, B. Wei, Y. Heng, C. Luo, X. Guo, and B. Cao, "Design of absorptive superconducting filter," *Electron. Lett.*, vol. 53, no. 11, pp. 728—730, May 2017.

[6] D. Psychogiou and R. Gómez-García, "Reflectionless adaptive RF filters: Bandpass, bandstop, and cascade designs," *IEEE Trans. Microw. Theory Techn.*, vol. 65, no. 11, pp. 4593–4605, Nov. 2017.

[7] L. Yang *et al.*, "Multilayered reflectionless wideband bandpass filters with shunt/in-series resistively terminated microstrip lines," *IEEE Trans. Microw. Theory Techn.*, vol. 68, no. 3, pp. 877–893, Mar. 2020.

[8] L. Yang, R. Gómez-García, M. Fan, and R. Zhang, "Multilayered input-reflectionless quasi-elliptic-type wideband bandpass filtering devices on diplexer-based structures," *IEEE Trans. Microw. Theory Techn.*, vol. 70, no. 1, pp. 122–138, Jan. 2022.